

Simulation of antiproton-nucleus interactions in the framework of the UrQMD model

A.S. Galoyan, A.Polanski

This paper proposes to apply the Ultra-Relativistic Quantum Molecular Dynamic (UrQMD) approach to implement the PANDA project (GSI). Modeling of $\bar{p}A$ -interactions has been performed at antiproton energies from 1 GeV to 200 GeV by using the UrQMD model. We have studied average multiplicities, multiplicity distributions of various types of secondary particles, correlations between the multiplicities, rapidity, and transverse momentum distributions of the particles. The UrQMD model predictions on inelastic $\bar{p}A$ - collisions have been found to reproduce qualitatively the experimental data. However, to reach the quantitative agreement, especially, in fragmentation regions, it is needed to modify the UrQMD model.

1 Introduction

In our paper we perform a comparative analysis of experimental data on $\bar{p}A$ -interactions with calculations using the well-known Ultra-Relativistic Quantum Molecular Dynamic model (UrQMD) [1].

The property of antinucleons - the ability to annihilate in nuclear matter, gives an ample possibility to investigate exotic nuclei and processes. The presence of an annihilation channel in the $\bar{N}A$ -interaction leads to enhancement of such interesting effects in intranuclear cascades as multipion-nucleus interactions and the interaction of meson resonance with nuclei [4]. This also may result in qualitatively new effects, for example, the formation of a droplet of "hot" nuclear matter [2], [3] with its subsequent specific decay. Specifically, in [5] it is shown that in the interaction of antiprotons with tantalum nuclei K_s^0 -particles are mainly produced from the cluster containing p+3 nucleons with temperature $T \approx 135$ MeV, and Λ -particles - from the cluster containing p+13 with temperature $T \approx 97$ MeV.

Analyzing the annihilation of antinucleons in nuclei, it is interesting, first of all, to determine the difference of the characteristics of secondary particles in the $\bar{p}A$ - interactions from the predictions of microscopic models for hadron-hadron and nucleus-nucleus collisions, in particular, Ultra-Relativistic Quantum Molecular Dynamic model (UrQMD), and from the data on nucleon-nucleus interactions for which the UrQMD model gives a qualitative agreement. The above mentioned specific features may be associated with the effect of clustering nucleons in the intranuclear annihilation process or, probably, some demerits of the model.

Our work has been inspired by the goals of the PANDA project at GSI. Among them there are those which are especially important for UrQMD contribution:

- Study of interactions of hidden and open charm particles with nucleons and nuclei;
- Investigation of strange baryons in nuclei.

To reach these goals, it is necessary to have \bar{p} -nucleus events code-generator

- to estimate the background conditions for experiment;

- to develop the experimental setup, trigger conditions, and so on.

Of course, the generator of \bar{p} -nucleus interactions is needed to study the physics of processes.

There are only few event generators – FLUKA [6], Intranuclear cascade model [7], DTUJET [8], UrQMD, to simulate \bar{p} -nucleus collisions. We assume that the UrQMD approach is the most suitable tool to solve these tasks.

2 Main assumptions of UrQMD approach

A detailed model description can be found in papers [1]. The UrQMD model is a microscopic transport theory based on the covariant propagation of all hadrons on classical trajectories in combination with stochastic binary scatterings, colour string formation and resonance decay.

It represents a Monte-Carlo solution of a large set of coupled partial integro-differential equations for the time evolution of various phase space densities $f_i(x, p)$ of particle species $i = N, \Delta, \Lambda$, etc, that non-relativistically assumes the Boltzman form:

$$\frac{df_i(x, p)}{dt} \equiv \frac{\partial p}{\partial t} \frac{\partial f_i(x, p)}{\partial p} + \frac{\partial x}{\partial t} \frac{\partial f_i(x, p)}{\partial x} + \frac{\partial f_i(x, p)}{\partial t} = Stf_i(x, p),$$

where x and p are the position and momentum of particle, respectively, $Stf_i(x, p)$ denotes the collision term of these particle species, which are connected to any other particle species $f_k(x, p)$.

The UrQMD approach includes

- consideration of cross-section of various meson-meson, meson-baryon, and baryon-baryon interactions. It takes into account ~ 50 baryons, ~ 45 mesons.
- It considers $Q\bar{Q}$ string creation a la FRITIOF model at $P_{lab} > 5\text{GeV}/c$.
- It also considers string fragmentation and formation time of particles.
- At lower energies, $P_{lab} < 5\text{GeV}/c$ there are reaction channels:
 $N + N \rightarrow \Delta N, \Delta\Delta, N^*N, \text{etc.}, M + N \rightarrow \Delta^0, \Lambda, \dots$
- The potential interactions are supposed between the particles, especially, Yukawa, Coulumb, Pauli potentials.

The physical picture of hA collisions, used by UrQMD model is approximately the following. The projectile hadron interacts with the target nucleus nucleon. A collision between two hadrons will occur if $d < \sqrt{\sigma_{tot}/\pi}$, where d and σ_{tot} are the impact parameter of hadrons and the total cross-section of two hadrons, respectively. In the UrQMD model the total cross-section σ_{tot} depends on the isospins of colliding particles, their flavor and the c.m.s. energy. However, partial cross-sections are then used to calculate the relative weights for different channels. The total baryon-baryon cross-section of the reaction $A + C \rightarrow D + E$ has the following general form:

$$\sigma_{tot}^{BB} \propto (2S_d + 1)(2S_E + 1) \frac{\langle p_{D,E} \rangle}{\langle p_{A,C} \rangle} \frac{1}{s} |M|^2,$$

with the spins of the particles, S_i , momenta of the pairs of particles, $\langle p_{i,j} \rangle$, in the two particle rest frame, and the matrix element $|M|^2$.

At high energies, two quark strings are produced in the hadron interaction with target nucleon. The first fast string can collide with other target nucleon or emit a meson(s), before the collision with the second nucleon of the target. The second string, slow in the Lab. system, decays in the nucleus and its products interact with the nuclear nucleons. Here, the creation of different meson and baryon resonances are taken into account. The resonances can interact with each other and nuclear nucleons, before they leave the nucleus. As a result, a lot of particles are produced in the simulated hA -interactions with UrQMD model.

At high energies ($p_{lab} > 2$ GeV/c) baryon-baryon and meson-baryon cross-sections are parameterized as:

$$\sigma_{tot,el}(p) = A + Bp^n + C\ln^2(p) + D\ln(p)$$

with the parameters of the CERN-HERA fit [9], the laboratory momentum p in GeV/c and the cross-section in mb. To describe the total meson-meson reaction cross-sections, the additive quark model (AQM) and the principle of detailed balance are used, that assumes the reversibility of the particles interactions. To model meson-meson interactions above the resonance region $\sqrt{s} > 1.7$ GeV, one applies the rescaled total πp cross section:

$$\sigma_{tot}^{MM}(\sqrt{s} > 1.7\text{GeV}) = \sigma_{tot}^{\pi p}(\sqrt{s}) \frac{\sigma_{AQM}^{MM}}{\sigma_{AQM}^{\pi p}}.$$

If we look at the Cascade model [10], it only considers the reactions:

$$NN \rightarrow NN + m\pi, \pi N \rightarrow \pi N, \pi N \rightarrow N + m\pi, \pi + (NN) \rightarrow NN.$$

As you can see, there are no ω , ρ -mesons, Δ -izobars, Λ -hyperons, etc. All of them are presented in the UrQMD approach. As a result, the model UrQMD describes the hadron-hadron and hadron-nucleus interactions quite well. To test this, we have considered experimental data on hadron-hadron and hadron-nucleus interactions.

In Fig. 1 we present experimental data and UrQMD model calculations on π^- -meson rapidity and transverse momentum distributions in neutron-proton interactions at the neutron momentum of $P_n = 1.25, 1.73, 2.23$ and 5.1 GeV/c [11]. The experimental data on np -interactions were obtained with the 1-meter hydrogen chamber of the Laboratory of High Energies (LHE), JINR, by a group of Yu.A. Troyan. The histograms are experimental data, the solid lines are calculations performed by means of the UrQMD model, the dashed lines are modified FRITIOF [12] model calculations. As seen in Fig. 1, the qualitative and quantitative description of π^- -meson characteristics was obtained by the UrQMD model and the modified FRITIOF model.

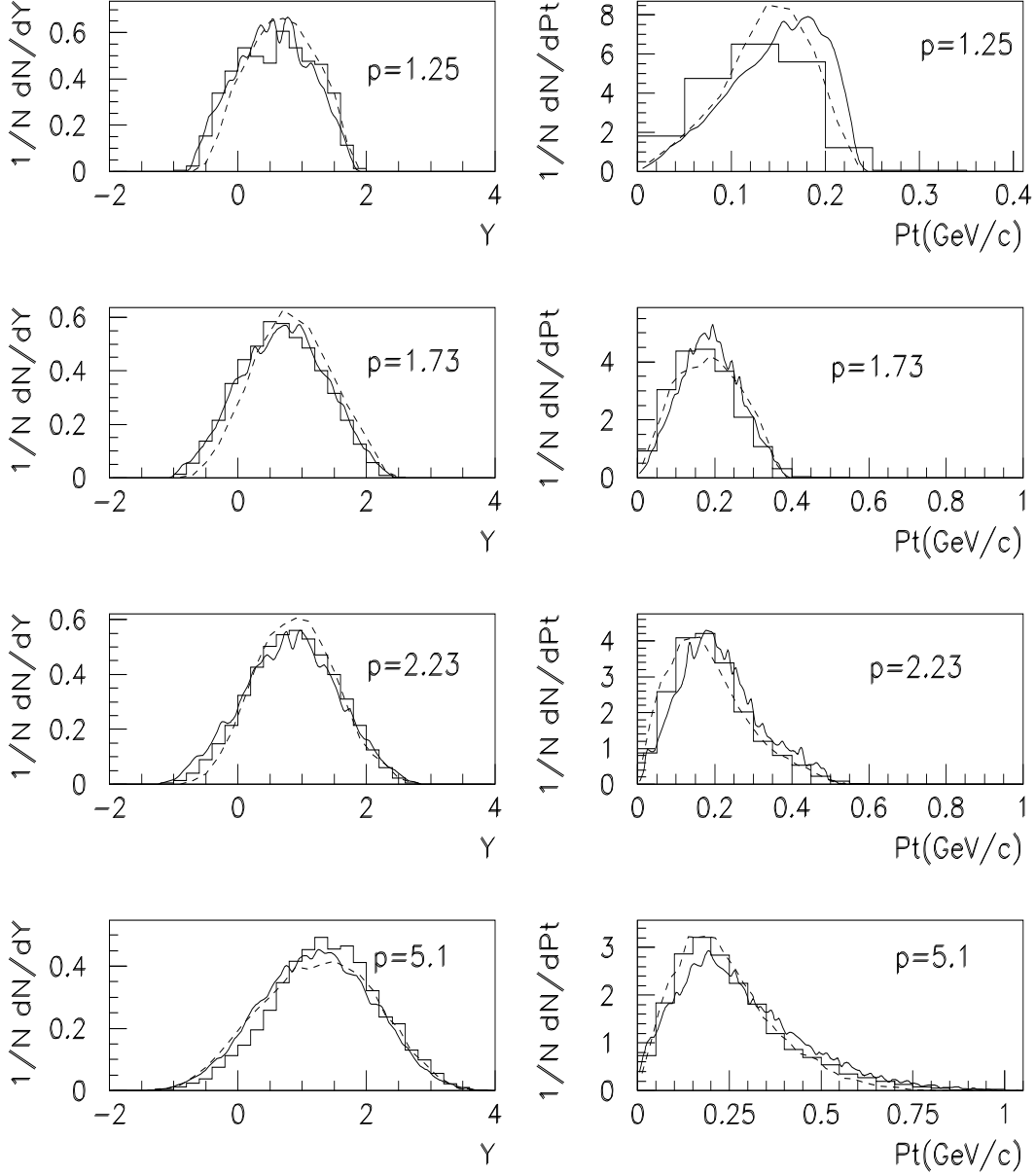


Figure 1: π^- meson rapidity and transverse momentum distributions in np -interactions. Histograms are experimental data [11]. Solid and dashed lines are UrQMD and modified FRITIOF [12] model calculations, respectively.

Fig. 2 gives experimental and model distributions of protons on transverse momentum in np -interactions in the reactions: $np \rightarrow pp\pi^-$ (Figs. 2a, 2d), $np \rightarrow pp\pi^-\pi^0$ (Figs. 2b, 2e), $pp \rightarrow np\pi^+\pi^-$ (Figs. 2c, 2f) at the neutron momentum of $P_n = 3.83$ GeV/c and 5.1 GeV/c. Histograms are the experimental data, solid lines are the UrQMD model calculations. Fig. 2 shows that the model predicts a larger yield of protons at small transverse momenta and underestimates their number at large momenta. However, the agreement of the calculations of transverse momentum distributions of protons in np -interactions with the experimental data is as satisfactory, as for π^- meson spectra.

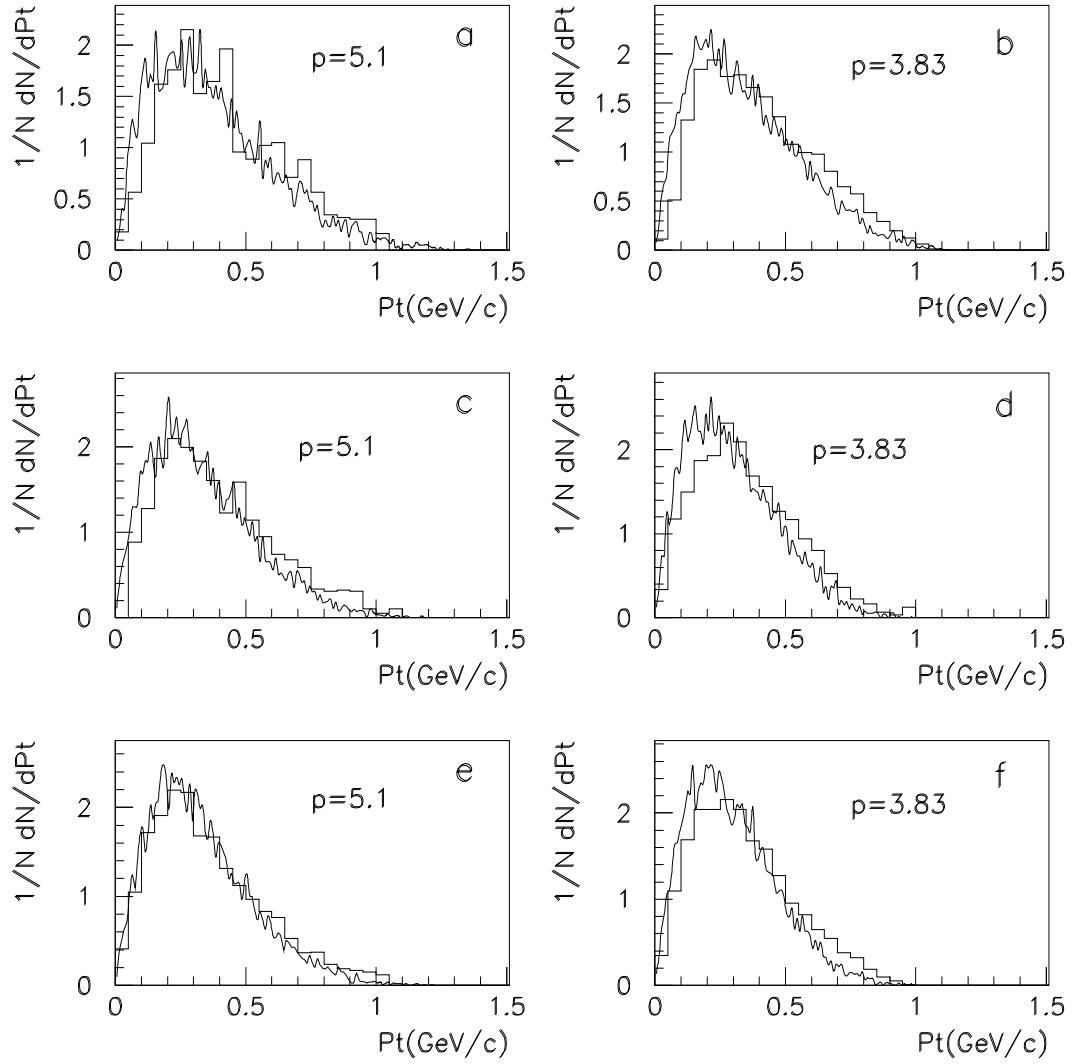


Figure 2: Proton transverse momentum distributions in np -interactions. Histograms are experimental data [11]. Solid lines are UrQMD model calculations.

Figs. 3, 4 present the data of pC -interactions at proton momentum of $P = 4.2$ GeV/c, obtained by means of the 2-meter propan bubble chamber of LHE, JINR. A method of receiving and developing data is described in Ref. [13], [14]. Fig. 3 depicts the multiplicity distributions of all charged particles, π^- and π^+ mesons, and participant protons with the momentum more than 0.3 GeV/c in pC -interactions. The points are experimental data, the solid, dashed and dotted lines are the UrQMD, modified FRITIOF [14] and cascade [10] model calculations, respectively. It is interesting, that the UrQMD model describes the participant proton spectra better than the modified FRITIOF and the cascade model, and for the other groups of particles three models give the same good agreement with experimental multiplicity distributions. Fig. 4 presents the kinematical characteristics of the secondary particles: participant protons with the momentum more than 0.3 GeV/c, π^- and π^+ mesons. The distributions of secondary particles on the rapidity and momentum are shown in Fig. 4. The UrQMD model calculation overestimates the production of π -mesons in the central rapidity region, and, especially, of the protons in the target fragmentation region. The same exceed of particle multiplicity in the target fragmentation region takes place in $\bar{p}A$ -nucleus interactions, as it will be shown below. As seen in Fig. 4, the UrQMD model calculations reproduce quantitatively the experimental momentum distributions of π -mesons. On the whole, the UrQMD model calculations are in agreement with experimental data of the pC -interactions, as it was expected.

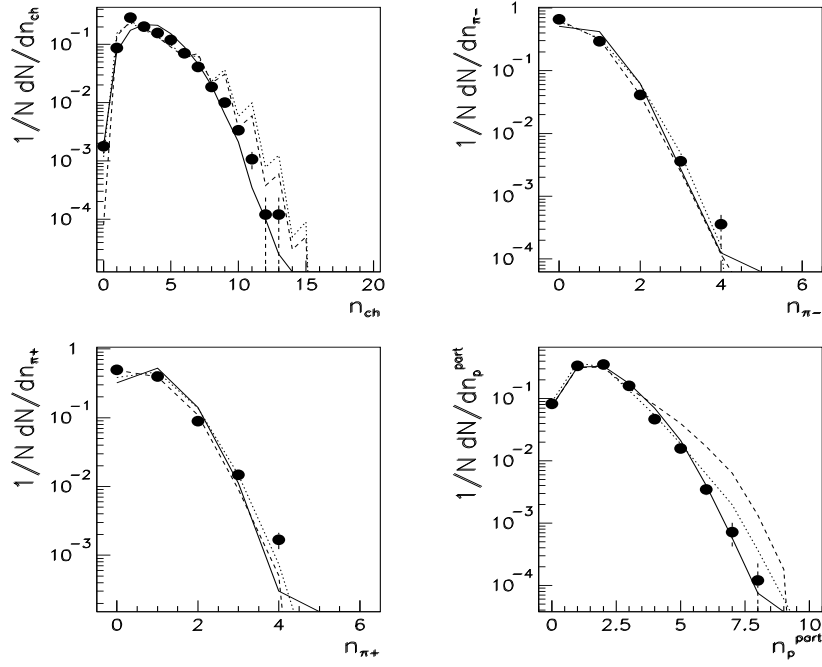


Figure 3: Secondary particles multiplicity distributions in pC-interactions. Points are experimental data [13], [14]. Solid, dashed and dotted lines are UrQMD, modified FRITIOF [14], and cascade [10] model calculations, respectively.

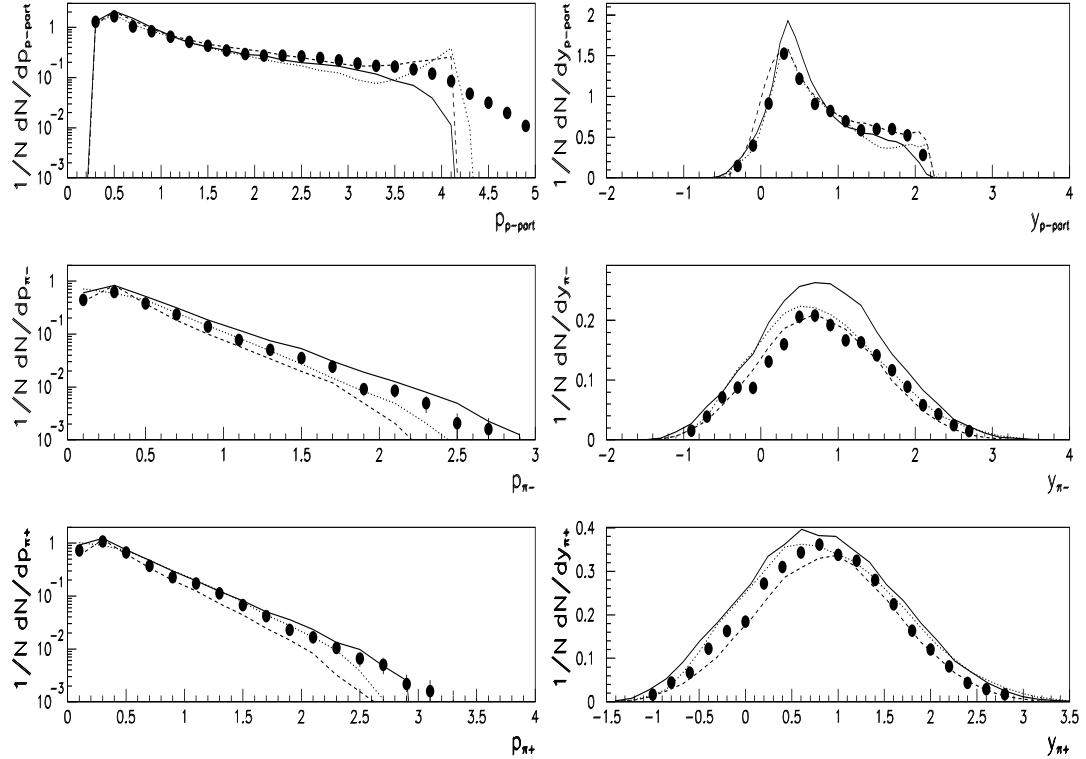


Figure 4: Secondary particles distributions on momentum (left side), on rapidity (right side) in pC-interactions. Points are experimental data [13], [14]. Solid, dashed and dotted lines are UrQMD, modified FRITIOF [14], and cascade [10] model calculations, respectively.

3 Results for $\bar{p}A$ -interactions and analysis

Antibaryon-baryon interactions are especially considered in the UrQMD approach. It is well-known that at the energies ≤ 100 GeV/c an important contribution to the total interaction cross-section comes from the annihilation process, where only mesons remain in the final state. In the model, the $\bar{p}p$ annihilation cross-section is parameterized by the relation taken from Koch and Dover [15]

$$\sigma_{ann}^{\bar{p}p} = \sigma_0^N \frac{s_0}{s} \left[\frac{A^2 s_0}{(s - s_0)^2 + A^2 s_0} + B \right]$$

with $\sigma_0^N = 120$ mb, $s_0 = 4m_N^2$, $A = 50$ MeV and $B = 0.6$. As known, the $\bar{n}p$ cross-section does not differ significantly from $\bar{p}p$ cross-section [16], hence, they are set equal in the UrQMD model. It is assumed, that two massive strings and one meson creation take place at the annihilation. Since the strings have practically the same energies and masses and are flying in the same direction, we can expect, that there is a double multiplicity of produced particles, compared with the multiplicity in NN -interactions. Since the interference between the particles is not considered in the UrQMD model, we can expect that there is a more powerful cascade compared with the cascade in hadron-nucleus interactions.

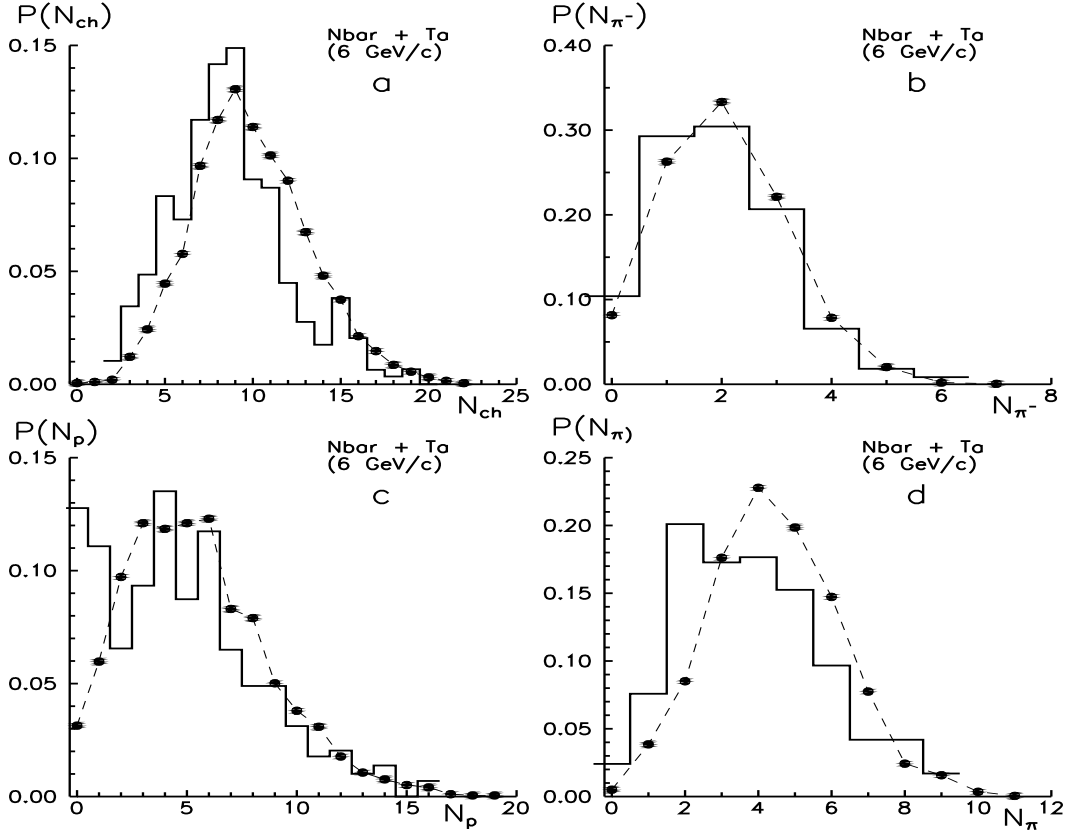


Figure 5: Multiplicity distributions of secondary particles: a) all charged particles, N_{ch} , b) negative charged particles, N_{π^-} , c) identified protons, N_p , d) charged mesons, N_{π} . Histograms are experimental data [19], points and dashed lines are UrQMD model calculations.

To check the expectation, we turn to the experimental data on \bar{p}, \bar{n} -interactions with nuclei. In the well-known "Guide to experimental particle physics literature" [17], [18], there are only few references on antibaryon-nucleus interactions in the energy range from 1 to 20 GeV/c [19], [20]. However, there are a lot of references on $\bar{p}A$ -interactions at energies 40 GeV/c, 100 GeV/c, 200 GeV/c.

In Fig. 5 we present the charged particles multiplicity distributions in $\bar{n}Ta$ -interactions at 6 GeV/c. The experimental data [19] were obtained by using the two-meter liquid-hydrogen chamber "LYUDMILA" of the LHE of the JINR. A tantalum target was placed in the active volume of the chamber, which was exposed to the beam of antideutrons at momentum 12.2 GeV/c in the accelerator of the Institute for High-Energy Physics at Serpukhov. The statistics of experimental data consists of 250 events. Our statistics includes 2000 events. Fig. 5a shows the multiplicity distribution of all charged particles, N_{ch} . In the experiment [19], the protons with momentum less than 1 GeV/c have been identified. Fig. 5c gives the multiplicity distribution of slow (identified) protons, N_p . Figs. 5b and 5d illustrate the multiplicity distribution of secondary negative charged particles, $N_{\pi-}$, and of all charged mesons, N_{π} , respectively. These so-called mesons (Fig. 5d) include all charged mesons and unidentified protons with momentum more than 1 GeV/c. As seen, there is a qualitative agreement between the experimental data and the theory.

	N_{event}	$\langle N_{ch} \rangle$	$\langle N_p \rangle$	$\langle N_{\pi} \rangle$	$\langle N_{\pi-} \rangle$	$\langle N_{\pi+} \rangle$
$\bar{n}Ta$	209	8.91 ± 0.24	4.93 ± 0.26	3.92 ± 0.14	1.97 ± 0.09	1.96 ± 0.09
UrQMD	2000	9.896	5.452	4.444	2.024	2.420
ICM	1000	8.12	2.91	5.21	2.57	—

Table 1: Average multiplicities of secondary charged particles in nTa -interactions at $P_{lab} = 6\text{GeV/c}$

Table 1 lists the considered experimental data [19] (the first line) and calculations of the average multiplicities of secondary charged particles for the interactions of antineutrons with tantalum nuclei at 6 GeV/c. We present the simulations in the framework of the UrQMD model (second line) and the intranuclear cascade model (ICM) [7] (third line). The average multiplicity of all charged particles, N_{ch} , calculated with the UrQMD model, overestimates the experimental one by 10%. The theoretical average multiplicity of identified protons, N_p , also exceeds the experimental one by 10%, the calculated multiplicity of the so-called π mesons, N_{π} , overestimates the experimental data by 13%, the simulated average multiplicity of negative charged particles, $N_{\pi-}$, differs from the experimental multiplicity only by 3%. The big difference is observed between the experimental data and UrQMD calculations on positive mesons and unidentified protons, $N_{\pi+}$, it reaches 22%. Table 1 illustrates the big discrepancy in the intranuclear cascade model calculations and experimental data, especially, for average multiplicity of identified protons. This difference equals $\sim 40\%$.

The correlations between multiplicities of mesons and identified protons give additional information on features of $\bar{n}Ta$ -interactions. Fig. 6 displays various experimental correlations between protons and pions with the corresponding UrQMD and ICM calculations. From Fig.6a one can see that the experimental average multiplicity of the identified protons (solid points) falls with increase of the pion production by $\sim 2.5 - 3$ times. The average multiplicity of π -mesons decreases with enhance of the identified protons yield (see Fig.6b) by \sim two times. On the whole, the UrQMD calculations (dashed lines and

open points) reproduce quite well the shape of the experimental correlations, but there is a quantitative discrepancy. At the same time, predictions of ICM (the histograms) differ very strongly from the experimental data (see Figs. 6a, 6b). Due to low statistics of this experimental data we cannot make a conclusion on the accuracy of calculations with the UrQMD model.

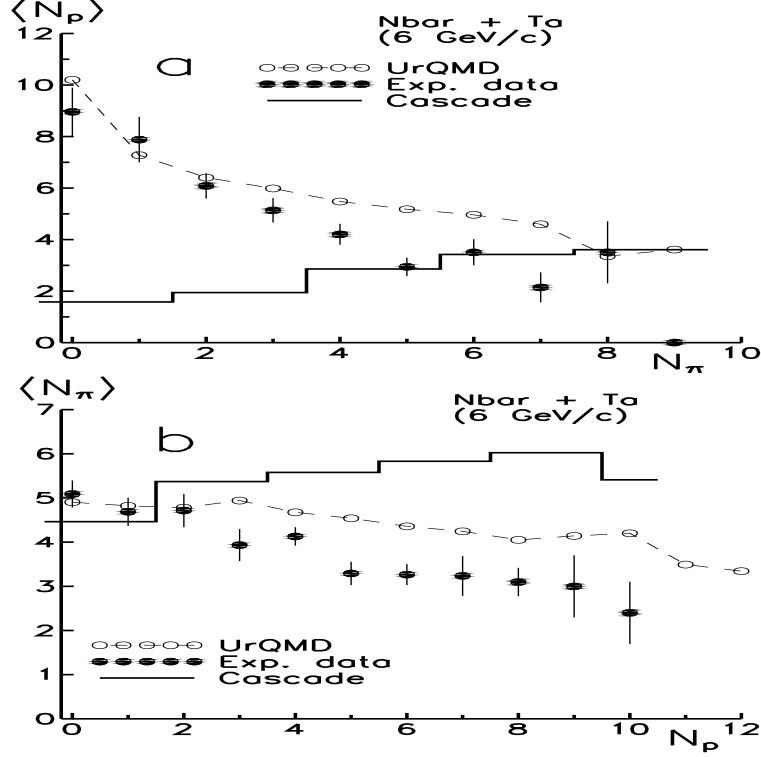


Figure 6: Correlations between protons and pions: a) dependence of the average number of protons, $\langle N_p \rangle$, on the number of pions, N_π , b) dependence of the average number of pions, $\langle N_\pi \rangle$, on the number of identified protons, N_p . Filled circles are experimental data [19], dashed lines and histograms are UrQMD and ICM [7] calculations, respectively.

Let us look at the experimental data [21], [22] on $\bar{p} + Li, C, S, Cu, Pb$ interactions at \bar{p} momentum of 40 GeV/c. These interactions were studied with the RISK-streamer chamber spectrometer. In Fig. 7, the average multiplicities of all charged particles, $\langle N_{ch} \rangle$, the negative charged particles, $\langle N_{neg} \rangle$, the slow, identified protons with momentum less than 500 MeV/c, $\langle N_p \rangle$, and fast protons, $\langle Q \rangle$, are given as functions of the atomic weight A . Since one cannot determine the number of fast protons exactly in the experiment [21], therefore, the multiplicity of the so-called fast protons is defined as: $Q = N^+ - N^- + 1 - N_p$, where $N^{+(-)}$ is the number of positive (negative) particles. For experimental data (square points), Fig 7b shows that the increase with A of the average number of slow (identified) protons is much stronger than the linear behaviour and can be parameterized as $\langle N_p \rangle = c \cdot A^\alpha$, where $\alpha \approx 0.62$. The high value of α indicates that the slow protons are governed by cascading and, probably, by an admixture of some evaporation protons (at the 10% level [21]). From Fig. 7d, it is obvious that the average number of fast protons, $\langle Q \rangle$, depends much weaker on A than $\langle N_p \rangle$. The overestimation of the UrQMD model simulations (dashed lines in Fig. 7) on the average multiplicities of all charged particles, grows while increasing the atomic weight A . This is also true for the negative particles average multiplicity, $\langle N^- \rangle$, and the mean number

of slow protons, $\langle N_p \rangle$. This exceeding can be explained by the larger cascading of intermediate particles in nuclear matter on the model UrQMD than it takes place in the reality.

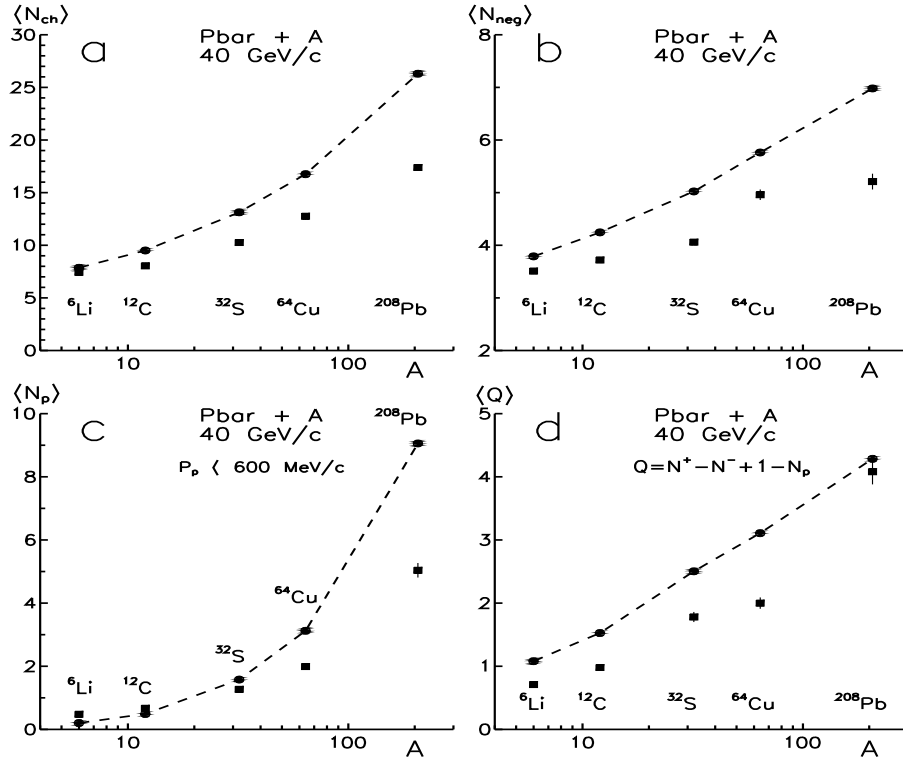


Figure 7: Average multiplicities of secondary particles: a) all charged particles, $\langle N_{ch} \rangle$, b) negative charged particles, $\langle N_{neg} \rangle$, c) identified protons, $\langle N_p \rangle$, d) fast protons, $\langle Q \rangle$, vs atomic weight. Squares are experimental data [21]. Dashed lines and circles are UrQMD model calculations.

Reaction		N_{event}	$\langle N_p \rangle$	$\langle N_{pb} \rangle$	$\langle Q \rangle$	$\langle N_{neg} \rangle$	$\langle N_{ch} \rangle$
$\bar{p}Li$	EXP	1156	0.48 ± 0.03	0.14 ± 0.02	0.71 ± 0.04	3.51 ± 0.05	7.43 ± 0.12
	UrQMD	3649	0.202	0.08	1.08	3.79	7.86
$\bar{p}C$	EXP	1113	0.67 ± 0.04	0.24 ± 0.02	0.98 ± 0.05	3.72 ± 0.10	8.04 ± 0.14
	UrQMD	4036	0.489	0.2	1.53	4.24	9.5
$\bar{p}S$	EXP	1135	1.27 ± 0.07	0.47 ± 0.03	1.78 ± 0.08	4.06 ± 0.10	10.26 ± 0.18
	UrQMD	4446	1.58	0.66	2.5	5.02	13.13
$\bar{p}Cu$	EXP	1419	1.99 ± 0.09	0.64 ± 0.04	2.00 ± 0.09	4.96 ± 0.10	12.76 ± 0.18
	UrQMD	4647	3.12	1.29	3.11	5.76	16.76
$\bar{p}Pb$	EXP	1108	5.04 ± 0.23	1.89 ± 0.11	4.08 ± 0.20	5.21 ± 0.15	17.39 ± 0.32
	UrQMD	3308	9.06	3.67	4.28	6.98	26.3

Table 2: Average multiplicities of secondary charged particles at $P_{lab} = 40 \text{ GeV/c}$

Table 2 shows that the disagreement reaches 60% for $\langle N_{ch} \rangle$, 40% for $\langle N^- \rangle$, and 80% for $\langle N_p \rangle$ for \bar{p} interaction with lead nucleus. The UrQMD model calculations considerably exceeds the average multiplicity of the identified protons, emitted in backward hemisphere, $\langle N_{pb} \rangle$, in Lab. system [22] for medium and heavy nuclei.

Let us consider experimental data [23] on $\bar{p}A$ -interactions at momentum of anytprotons 100 GeV/c. This experiment was performed with the Fermilab 30-inch bubble chamber and Downstream Particle Identifier to study inclusive charged pion production in the

high energy interactions of π^\pm , K^\pm , p and \bar{p} with thin foils of magnesium, silver and gold. The laboratory rapidity and transverse momentum distributions are presented separately for π^+ and π^- production and compared with the VENUS string model Monte Carlo in Ref. [23]. Laboratory rapidity is defined as

$$y = \frac{1}{2} \ln \left(\frac{E + P_z}{E - P_z} \right),$$

where E and P_z are the laboratory energy and longitudinal momentum, respectively.

We have performed the modeling of the reactions

$$\bar{p} + Mg, Ag, Au \rightarrow \pi^\pm + X \quad (1)$$

at momentum 100 GeV/c in the framework of the UrQMD model. Figs. 8, 9 show the results of the modeling and the corresponding experimental data [23].

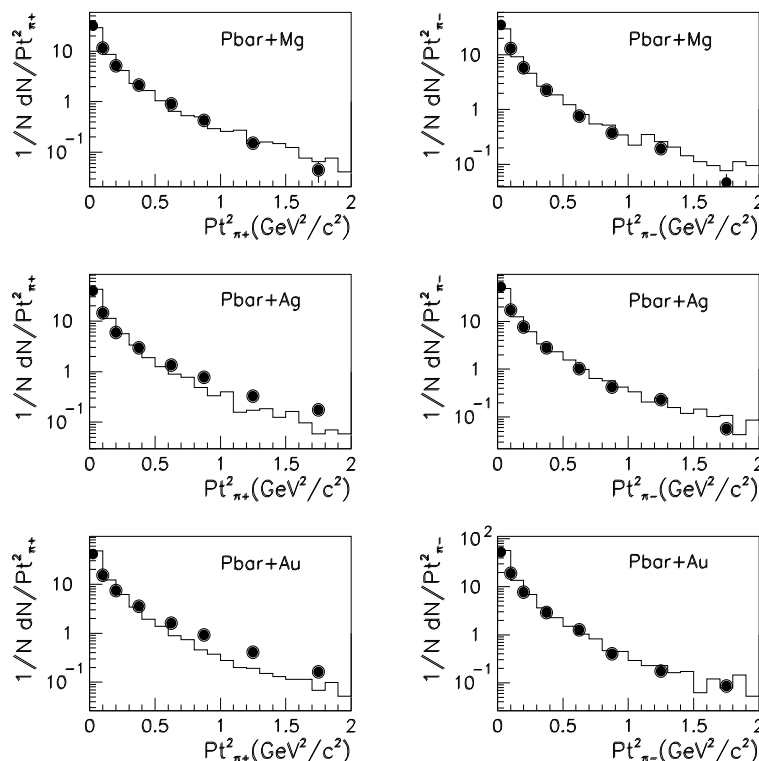


Figure 8: P_t^2 distributions of π^+ and π^- produced in $\bar{p}A$ -interactions at antiproton momentum 100 GeV/c. Solid points are experimental data [23]. Histograms are UrQMD model calculations.

Fig. 8 illustrates the transverse momentum distributions of π^+ and π^- - mesons. All of the spectra are similar in shape, but the Au data have slightly higher cross sections due to the higher charged particle multiplicities (see Table 3), and the Mg data have the smallest cross sections. All of the data show distributions which are inconsistent with a single exponential slope but could be fitted with the sum of two exponential distributions. The UrQMD model calculations reproduce the experimental transverse momentum distributions of pions, even in the regions of large P_t , which are not described correctly with most of Monte Carlo models. In Fig. 9 we plot the pion rapidity distributions for all reactions (1). All of the plots are similar and display the following features. We observe that in the backward direction ($y < 2$) they rise rapidly with increasing A . As the rapidity

increases, the A dependence becomes weaker and in the region $y \approx 4.5$ the distributions become almost independent of A . We also do not observe any region where a rapidity plateau exists.

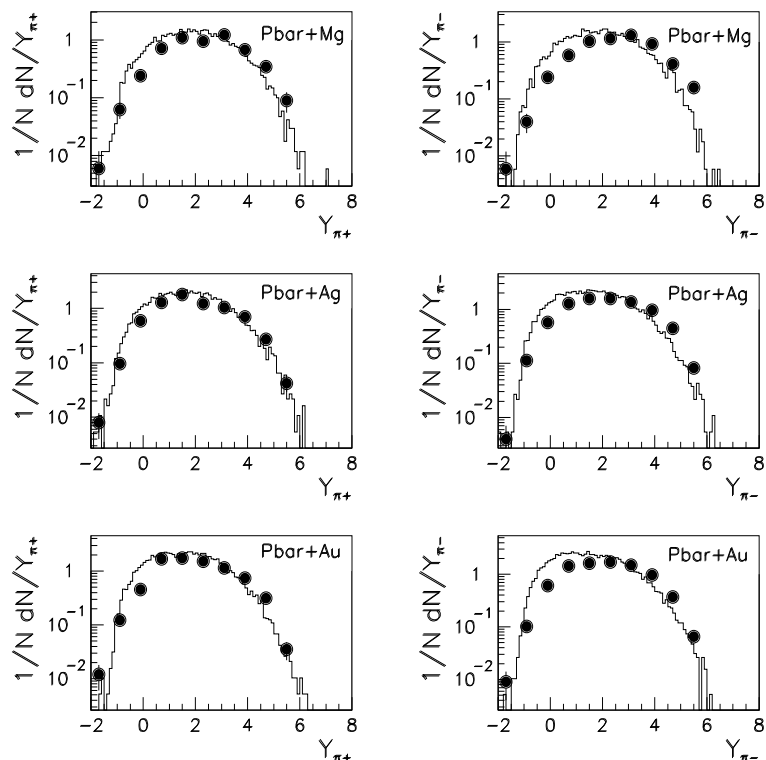


Figure 9: Rapidity distributions of π^+ and π^- produced in $\bar{p}A$ -interactions at antiproton momentum 100 GeV/c. Solid points are experimental data [23]. Histograms are UrQMD model calculations.

The UrQMD model simulations shift (a little bit) the rapidity distributions of π^+ and π^- mesons to the target fragmentation region. On the whole, the agreement between UrQMD and data [23] is reasonably good. Let us note, that the UrQMD model describes the π^+ and π^- kinematical spectra better than the VENUS model. In particular, the Venus model calculations strongly underestimate the yield of pions in the central rapidity region, and decrease essentially the meson production at large P_t (see [23]).

reaction		N_{event}	$\langle N_{\pi^+} \rangle$	$\langle N_{\pi^-} \rangle$
$\bar{p}Mg$	EXP	218	4.30 ± 0.19	4.68 ± 0.16
	UrQMD	1701	5.12	5.49
$\bar{p}Ag$	EXP	582	5.63 ± 0.15	6.41 ± 0.11
	UrQMD	1841	7.05	7.96
$\bar{p}Au$	EXP	465	6.24 ± 0.16	6.71 ± 0.13
	UrQMD	1906	7.8	9.09

Table 3: Average multiplicities of secondary charged particles at $P_{lab} = 100\text{GeV}/c$

However, the average multiplicity of π^+ and π^- mesons produced in $\bar{p}A$ -interactions at 100 GeV/c calculated with UrQMD considerably overestimates the experimental ones, as it was observed for the reactions $\bar{p}A$ at 40 GeV/c.

Table 3 presents the experimental and the UrQMD model calculated average multiplicity of π^+ , $\langle N_{\pi^+} \rangle$, and π^- , $\langle N_{\pi^-} \rangle$, produced in the reactions $\bar{p} + Mg$, Ag , Au at momentum of antiprotons 100 GeV/c. For Mg and Ag targets, the difference between the UrQMD calculations and experimental results is equal to $\sim 20\% - 25\%$, and $\sim 30\% - 35\%$ for Au target.

A similar situation with the multiparticle production in the $\bar{p}A$ -interactions takes place at momentum 200 GeV/c. Table 4 lists experimental data [24] and calculations by the UrQMD approach on the number of events, the average multiplicities of all charged particles, $\langle N_{ch} \rangle$, the negative particles, $\langle N_{neg} \rangle$, the forward emitted particles in the CMS system, $\langle N_F \rangle$, and the backward ones, $\langle N_B \rangle$ for $\bar{p}p$, $\bar{p}Ar$, $\bar{p}Xe$ interactions at the 200 GeV/c antiproton beam.

Reaction		N_{event}	$\langle N_{ch} \rangle$	$\langle N_{neg} \rangle$	$\langle N_F \rangle$	$\langle N_B \rangle$
$\bar{p}p$	Exp.	1856	7.69 ± 0.09	3.90 ± 0.05	3.97 ± 0.06	3.56 ± 0.06
	UrQMD	5000	6.009	3.003	3.277	2.732
$\bar{p}Ar$	Exp.	577	16.01 ± 0.40	6.80 ± 0.16	5.45 ± 0.12	8.97 ± 0.29
	UrQMD	1896	19.243	8.083	5.205	14.038
$\bar{p}Xe$	Exp.	905	22.41 ± 0.46	8.54 ± 0.15	6.19 ± 0.10	12.75 ± 0.33
	UrQMD	4694	29.061	10.386	5.642	23.419

Table 4: Average multiplicities of secondary charged particles at $P_{lab} = 200 \text{ GeV/c}$

The interactions of 200 GeV antiprotons on hydrogen, argon and xenon were studied with the streamer chamber vertex spectrometer [24] at the CERN SPS. Let us note, that the UrQMD model predicts low multiplicities for all and negative charged particles in $\bar{p}p$ -collisions. At the same time, the model gives a larger multiplicity of particles for \bar{p} interactions with heavy nuclei compared with experimental data. As seen from Table 4, the UrQMD model calculations reproduce quite well the experimental values of the average multiplicities of particles emitted in a forward hemisphere. The disagreement between the theory and the experimental data on the average multiplicity of the backward particles reaches 80% for $\bar{p}Xe$ -interactions.

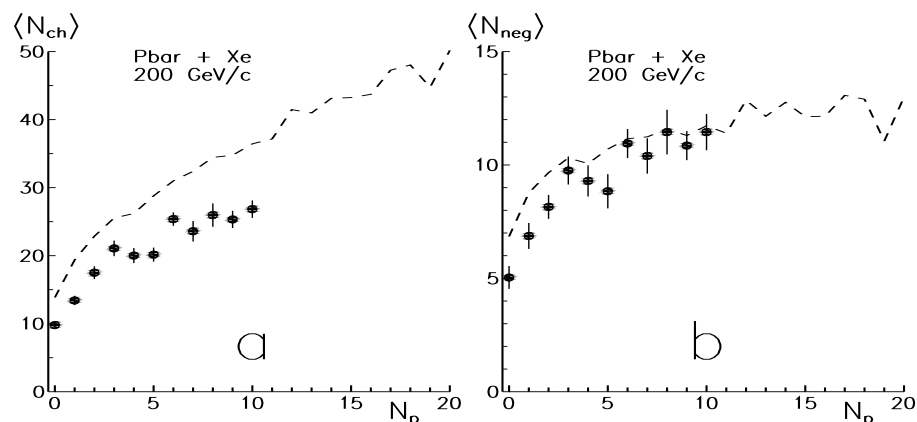


Figure 10: Correlations between protons and pions: a) dependence of the average number of all charged particles, $\langle N_{ch} \rangle$, on the number of identified protons, N_p , b) dependence of the average number of negative charged particles, $\langle N_{neg} \rangle$, on the number of protons. Circles are experimental data [24], dashed lines are UrQMD calculations, respectively.

Figs. 10a, 10b show the average multiplicity of produced particles N_{ch} and negative particles N_{neg} in $\bar{p}Xe$ -events versus the number N_p of identified protons with the momentum less than 600 MeV/c. At high values of N_p the average multiplicity has a value by about three times more than that at $N_p = 0$. Fig. 10 illustrates the both average multiplicity of charged particles and negative particles rise with enhance of the identified proton number. The corresponding UrQMD model calculations reproduce the experimental correlations qualitatively, but there is a quantitative difference between the simulations and the data for dependence of the average multiplicity of all charged particles on the number of the identified protons. The number of identified protons in simulations can be more than 20. At the same time, the number N_p in experiment reaches only 10.

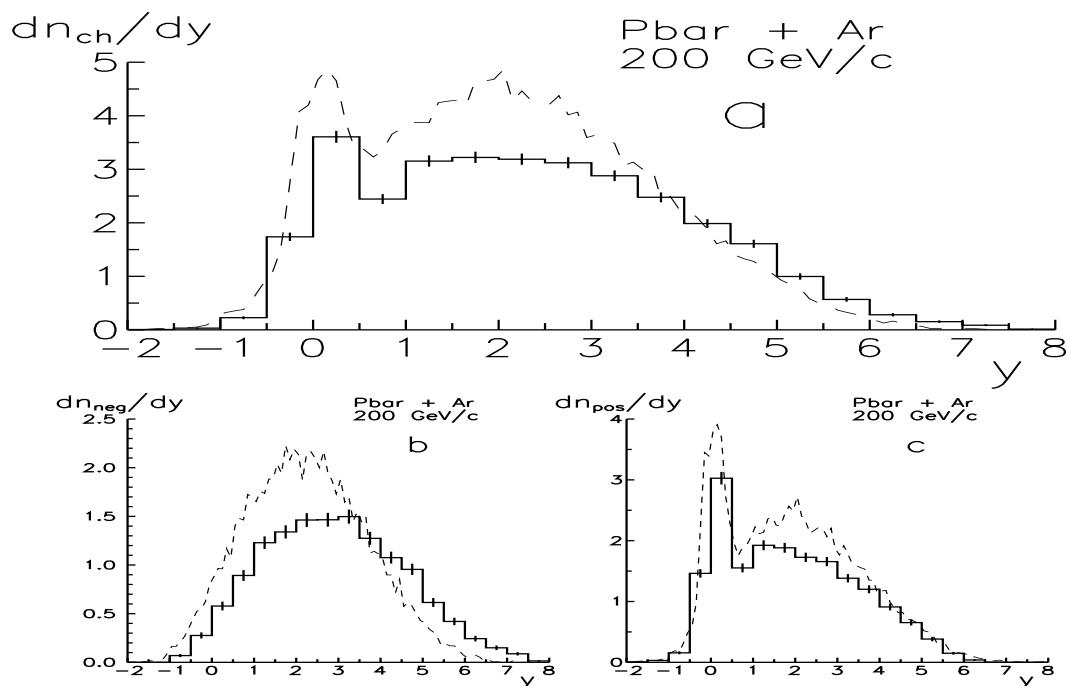


Figure 11: Rapidity distribution of charged particles in $\bar{p}Ar$ -interactions: a) all charged particles, b) negative charged particles, c) positive charged particles. Histograms are experimental data [24], dashed lines are UrQMD model calculations.

Rapidity distributions of all, negative and positive charged particles give more detail information about the accuracy of model predictions. In Fig. 11 we present the rapidity distributions of secondary particles in $\bar{p}Ar$ -interactions at 200 GeV/c. In the rapidity distributions of all and positive charged particles, the peak at $y \sim 0$ is associated with fast ejected target protons or with dissociation of the protons.

The following observations can be made:

- The UrQMD model assumes dominant production of all charged particles in the central rapidity region and in the target fragmentation region.
- The model gives a shift of the negative particle rapidity distribution to the target fragmentation region.
- The model overestimates the multiplicity of positive charged particles in the central and the target fragmentation regions.

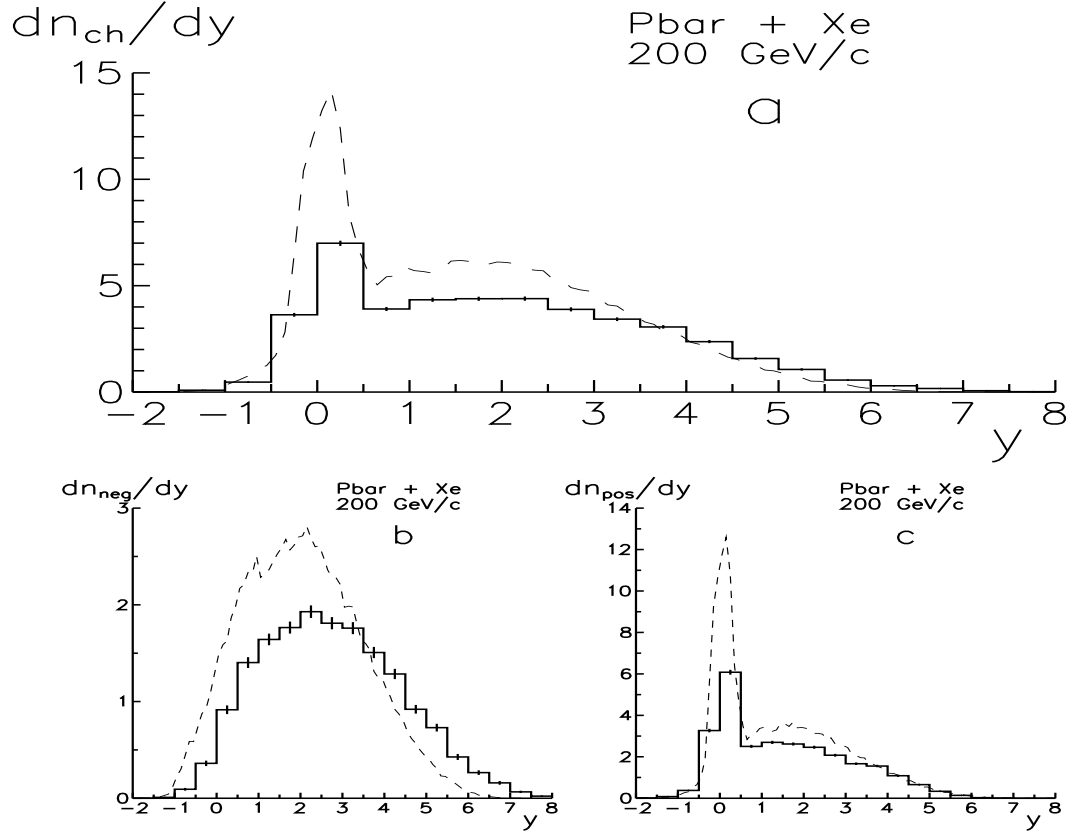


Figure 12: Rapidity distribution of charged particles in $\bar{p}Xe$ -interactions: a) all charged particles, b) positive charged particles, c) negative charged particles. Histograms are experimental data [24], points with dashed lines are UrQMD model calculations.

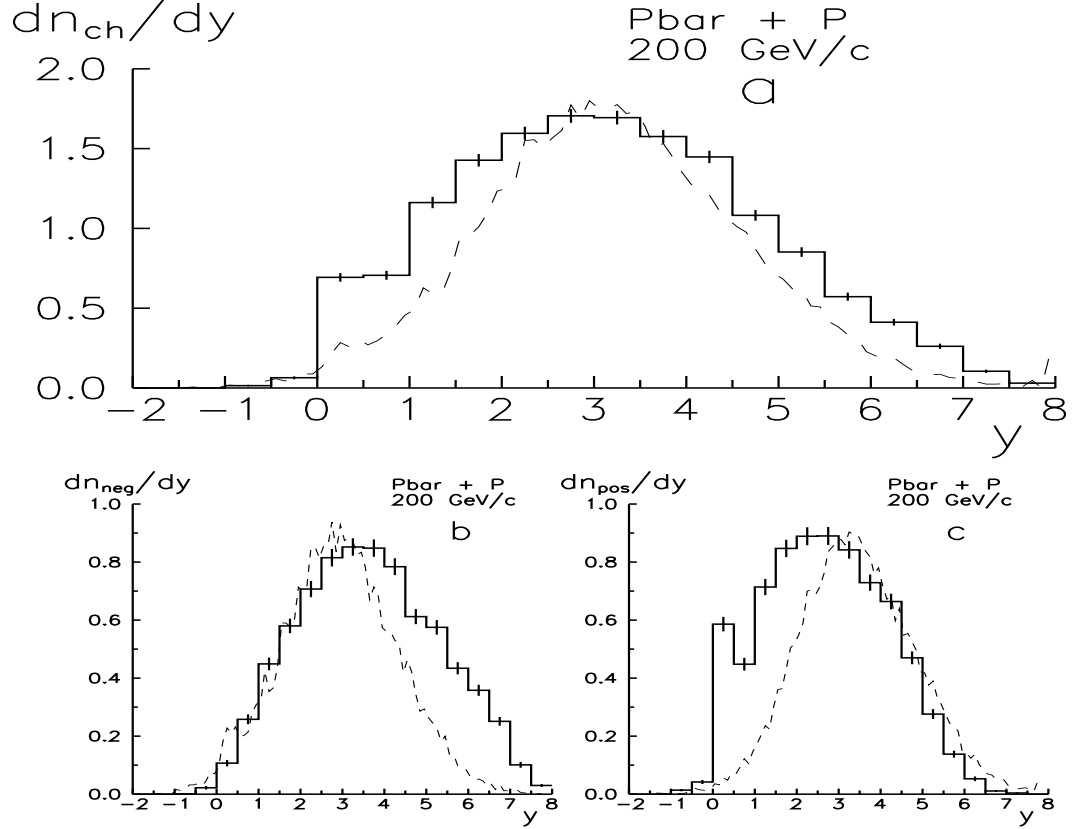


Figure 13: Rapidity distribution of charged particles in $\bar{p}p$ -interactions: a) all charged particles, b) positive charged particles, c) negative charged particles. Histograms are experimental data [24], points with dashed lines are UrQMD model calculations.

The same features are also presented in $\bar{p}Xe$ -interactions at momentum of the antiprotons at 200 GeV/c (Fig. 12). However, discrepancy between the calculated and experimental spectra in the central region and target fragmentation regions is essentially larger than in $\bar{p}Ar$ -interactions. It can be explained by effects of powerful cascading and a large number of produced resonances in the model $\bar{p}Ar$ -simulations.

The data of $\bar{p}p$ -interactions on rapidity distributions (see Fig. 13) show that the UrQMD approach does not describe the target and projectile fragmentation regions. There is a clean effect of \bar{p} leading and target proton leading in the experiment. However, the UrQMD approach assumes the central production of the charged particles, and there is no manifestation of the leading effect. Thus, we can conclude that the UrQMD approach does not consider diffraction dissociation quite correct.

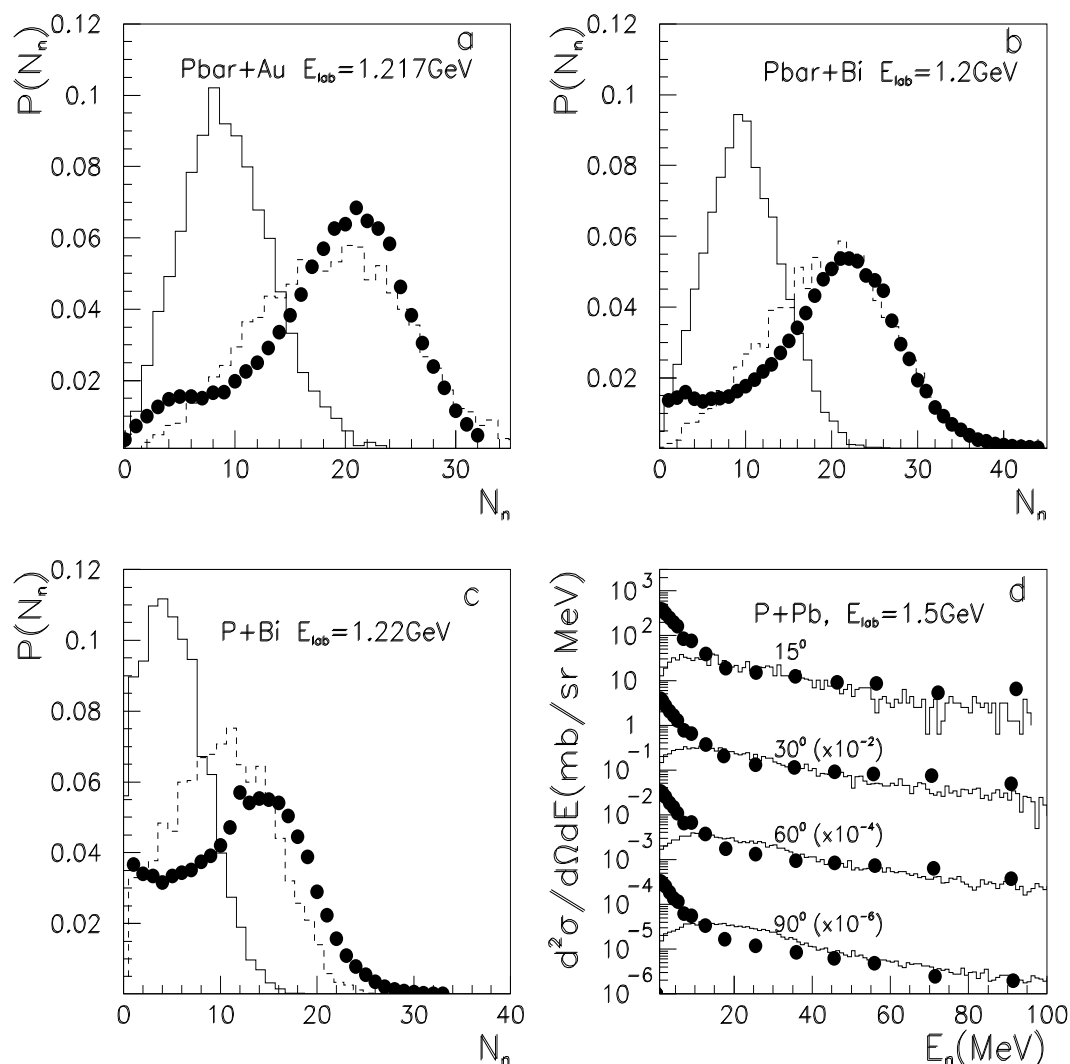


Figure 14: Multiplicity and energy distributions of produced neutrons in \bar{p}/p A-interactions: a) multiplicity distribution of neutrons produced in $\bar{p}Au$ -interactions, b) the same as in Fig. a for $\bar{p}Bi$ -collisions, c) the same as in Fig. a for pBi -interactions. Points are experimental data [20], solid and dashed lines are the UrQMD model calculations corrected and uncorrected for neutron detection efficiency, respectively. d) Energy distribution of neutrons produced at angles $15^\circ, 30^\circ, 60^\circ, 90^\circ$ in pPb -interactions. Points are experimental data [26], solid lines are the UrQMD model calculations.

In order to complete the consideration of the UrQMD model predictions, we have to analyse the products of nuclear residuals. To estimate radiation conditions of experiments, it is very important to know the multiplicity and energy spectra of neutrons produced by nucleus target in $\bar{p}A$ -interactions. Thus, we start with the multiplicities of neutrons produced in $\bar{p}Au, \bar{p}Bi, pBi$ -interactions at the energy of projectile baryons 1.2 GeV. Figs. 14a, 14b, 14c give experimental data [20] and calculation by the UrQMD model of the neutron multiplicity distributions. It is not clear from Ref. [20], whether the efficiency of the neutron detection by the Berlin Neutron Ball (BNB) [25] is taken or not into account in the experimental neutron multiplicity distribution. Therefore, we have shown both calculations uncorrected and corrected for neutron detection efficiency (dashed and solid lines in Figs. 14a, 14b, and 14c, respectively). The neutron detector BNB counts the number of neutrons with efficiency $\sim 80\%$ in the evaporation energy regime. For higher neutron energy, BNB detection efficiency drops to 30 – 40 % for pre-equilibrium neutron emission [25].

As seen, the essential missing of neutrons takes place in the simulations corrected for the neutron efficiency. The decrease of the produced neutron number is caused by the absence of the nucleus evaporation mechanism in the UrQMD model. To demonstrate this, we show the energy spectra of neutrons produced in pPb -collisions at the proton energy of 1.5 GeV. In Fig. 14d, the neutron energy distributions [26] at the laboratory angles of emitted neutrons $15^\circ, 30^\circ, 60^\circ, 90^\circ$ are exposed. As seen from Fig. 14d, at the neutron energy variation from 15 MeV to 1 MeV the calculated numbers of neutrons (solid lines) decrease. At the same time, the experimental spectra (points) grow up. Such slow neutrons are produced mainly in the processes of target nucleus evaporation. The underestimation of the multiplicities of the neutrons is at the level of $\sim 15 - 25$. We believe that it is needed to add the nucleus evaporation mechanism in the UrQMD model for accurate estimation of the kinematic characteristics of secondary neutrons. It is also observed that the UrQMD model predicts correctly the energy spectra of the pre-equilibrium, fast neutrons (see Fig. 14d).

Summing up, we conclude that the predictions of the UrQMD model agree qualitatively with the experimental data on $\bar{p}A$ -interactions. However, we believe that the accuracy of the UrQMD model predictions is not sufficient to estimate the background conditions for the experiment. The UrQMD model should be modified for a quantitatively description of the experimental data on $\bar{p}A$ -interactions.

The authors have benefited from instructive discussions with V.V. Uzhinsky, E.A. Stokovsky and J. Ritman.

References

- [1] S.A. Bass et al., Prog. Part. Nucl. Phys., 41, 1998, P. 225;
M. Bleicher et al., J.Phys. G25, 1999, P. 1859.
- [2] J. Rafelski Phys. Lett. 1980. V. 91B, P. 281.
- [3] J. Rafelski et al. CERN preprint TH. 2912, 1980.
- [4] A.S. Iljinov et al. Nucl. Phys. 1982. V. A382, P. 378.
- [5] K. Miano et al. Phys. Rev. Lett. 1984. V. 53, P. 1725.

- [6] J. Ranft, J.T. Routti, Comput. Phys. Commun. V. 7, 1974, P. 327.
- [7] Ye.S. Golubeva et al. Nucl. Phys. 1988. V. A483. P. 539.
- [8] P. Aurenche, et al., Comput. Phys. Commun., V. 83, 1994, P. 107.
- [9] Particle Data Group, Phys. Rev. D 54, 1996.
- [10] V.S. Barashenkov, V.D. Toneev "Interactions of high energy particles and nuclei with nuclei", Moskow, Atomizdat, 1972;
V.S. Barashenkov, F.G. Geregy, Zh.Zh. Musulmanbekov JINR Commun., P2-83-117, Dubna 1983.
- [11] A.Galoyan et al., JINR Preprint, E1-2001-68, Dubna 2001;
B.Ganhyayag, V.V. Uzhinskii, JINR Preprint, P1-97-315, Dubna 1997.
- [12] M.I. Adamovich et al., Zeit. für Phys., 1997, V. A358, P. 337;
V.V. Uzhinsky, JINR Preprint 2-81-780, Dubna 1981.
- [13] A.I. Bondarenko et al., JINR Communication, 1999, P2-99-59, Dubna 1999.
- [14] A. Galoyan et al., JINR Preprint P1-2002-54, Dubna 2002; A. Galoyan et al., JINR Preprint P1-2002-219, Dubna 2002; A. Galoyan et al., hep-ex/0208032.
- [15] P. Koch and C.B. Dover, Phys. Rev. C40, 145, 1989.
- [16] T. Elioff et al., Phys. Rev. 128, 869, 1962.
- [17] A Guide to Experimental Particle Physics Literature 1991-1996, LBL-90 Revised, UC-414, October 1996.
- [18] A Guide to Experimental Particle Physics Literature 1994-1998, LBL-90 Revised, October 1999.
- [19] V.F.Andreev et al., Sov. J. Nucl. Phys., V. 55, No 5 1990, P. 1275;
V.F.Andreev et al., Nuovo Cimento, V. 103A, No 8, 1989.
- [20] U. Jahnke et al., Sov. J. Nucl. Phys., V. 59, N. 9, P. 1625;
F. Goldenbaum et al., Phys. Rev. Lett., V. 77, N. 7, P. 1230.
- [21] E.G.Boos et al., Zeit. fur Phys., C26, 1984, P. 43.
- [22] L.L.Gabunia et al., JINR Prepint, P1-86-520, Dubna 1986.
- [23] J.J. Whitmore et al., Z. Phys. C 62, 1994, P. 199.
- [24] De Marzo et al., Phys. Rev., D26, 1982, P. 1019.
- [25] D. Hilscher, F. Goldenbaum et al., in Proceedings of the International Workshop on Nuclear Methods for Transmutation of Nuclear Waste, Dubna, edited by M.Kh. Khankhasayev, H.S. Plendl, and Z.B. Kurmanov (World Scientific, Singapore, 1997), P. 176.
- [26] K. Ishibashi et al., J. Nucl. Sci. Technol., 32, 1995, P. 827.